ANALYSIS OF POLARIZATION ORIENTATION ANGLE SHIFT ON HIGH RESOLUTION SPACEBORNE X-BAND AND C BAND SAR DATA

Shubham Awasthi[1], Shashi Kumar[2] and Praveen K Thakur[3]
[1,2] Photogrammetry and Remote Sensing Department
[3]Water Resources Department
[1,2,3]Indian Institute of Remote Sensing, Dehradun, Uttarakhand, India
Email: [1]shubahm.iirs@gmail.com, [2]shashi@iirs.gov.in,[3]praveen@iirs.gov.in

KEY WORDS: Synthetic aperture radar (SAR), Polarization orientation angle (POA), Fully Polarimetric data, Yamaguchi decomposition, POA compensation

ABSTRACT: The angle which formed between semi major axis of the polarized wave and the horizontal axis along the line of sight of the travelling microwave emitted from the sensor is called as the polarization orientation angle (Iribe, Sato, & Member, 2007). When the microwave strikes any irregular target surface the Polarization orientation angle (POA) shift occurs. This leads to the misinterpretation of the features after implementing decomposition modelling. This study focuses on analysis of Polarization Orientation Angle (POA) shift using high resolution spaceborne datasets. . The effect of Polarization orientation angle (POA) shift was analyzed on multi-frequency datasets. The fully polarimetric datasets of spaceborne sensors RADARSAT-2 and TerraSAR-X operating in the X-band and C band respectively were used. The datasets were acquired for the dates 12Feb 2015 and 24 Feb 2015 of the Bias river basin area situated in Manali region of Himachal Pradesh The decomposition techniques were implemented and variation in the outcomes with and without Polarization orientation angle (POA) shift compensation was observed. It was concluded that while implementing the decomposition model without any POA shift compensation volume scattering was overestimated however double bounce and surface scattering is underestimated. The POA shift observed in the Radarsat-2 datasets was greater compaired to the TerraSAR-X datasets. Hence it was concluded from the study that the sensor datasets operating in the low frequency experience more POA shift as compaired to the datasets at high frequency region.

1. INTRODUCTION

Microwave remote sensing using synthetic aperture radar is an advanced remote sensing technique. The polarized electromagnetic waves in the microwave region is utilized. The polarization channel diversity is used to transmit the electromagnetic waves in multi-polarizations simultaneously. SAR is capable of providing complex data with high spatial and temporal resolution in the all-weather conditions. It has the uniqueness of clouds and haze penetration while operating in the high frequency regions (Woodhouse, 2005), therefore is advantageous over optical remote sensing. Microwave remote sensing also has the property of penetration inside the dielectric medium and is sensitive to the dielectric properties of the medium (Fung & Chen, 2010).

The microwave backscattering is effected by the physical and geometrical properties of the targets. Polarizations channels used in microwave remote sensing are sensitive to different scattering mechanisms (Freeman & Durden, 1998; Raney, 2007; Yamaguchi, Moriyama, Ishido, & Yamada, 2005). Hence SAR polarimetry can be utilized for the classification of different targets based on their scattering mechanisms. Various decomposition modeling techniques are applied to classify the features inside the SAR resolution cell. The coherent and incoherent modeling techniques are applied based on weather the features inside a complex pixel is pure or mixed which has to be classified. The Lexicographic and Pauli techniques are coherent decomposition approaches, which are applied for the classification of the pure pixels. The Freeman and Yamaguchi techniques has the potential to classify the mixed pixels (Freeman & Durden, 1998; Yamaguchi et al., 2005). But few effects lead to the misclassification and wrong interpretation of the target features. When the imaging is done of the undulating rugged terrain areas the microwave experiences the polarization orientation angle(POA) shift. This POA shift effects the polarization state of the emitted electromagnetic wave. The horizontal field vector in the emitted electromagnetic wave from the microwave sensor is parallel to the incidence plane but due to the tilted

target surface in the undulating rugged terrain region, the horizontal vector is no longer parallel to the horizontal ground surface. Therefore the horizontal and vertical polarizations vectors are no longer mutually perpendicular to each other (Lee et al., 2002). Hence, the overall shift in the polarization orientation angle is experienced which can be easily represented by the polarization ellipse. This study focuses on the analysis of the polarization angle orientation shift on multi-frequency L band and X band spaceborne SAR datasets. The Radarsat-2 and TerraSAR-X datasets are utilized for this study. The POA shift in both the datasets is retrieved and frequency dependence of the POA shift is done using histogram analysis. The Yamaguchi decomposition technique before and after POA shift is applied and variation in different scattering mechanisms-surface, double bounce and the volume scattering is investigated.

2. STUDY AREA AND DATASETS USED

2.1 Study Area

The Beas River Basin up to Manali town with area of 350.21 km^2 has been selected for this study, in the state of Himachal Pradesh situated in Northern India. Area is at an altitude of 4350m above mean sea level, 51km north of Manali. The terrain is relatively undulating and is a part of North-Western Himalayas. The figure-1 below shows the map of the study area.

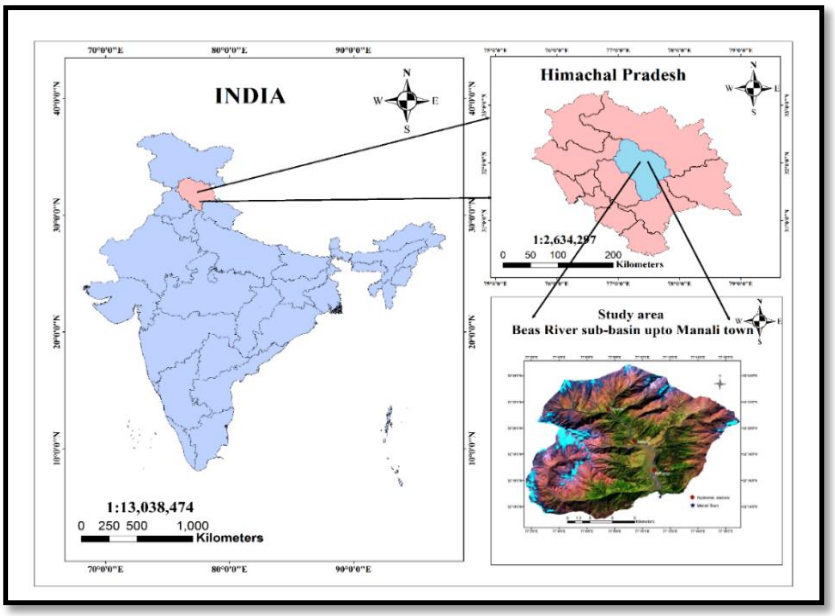

Figure 1-Study Area

2.2 Datasets Used

The multi-frequency quad-pol datasets of TerraSAR-X and Radarsat-2 sensors was used for this study. The datasets were acquired for the dates 21Jan-2015 and 25-Feb-2015 respectively. The detailed description of the used datasets is given in the table-1 below.

Data Specification	TerraSAR-X Datasets	Radarsat-2 datasets
Date of Acquisition	21-Jan-2015	25-Feb-2015
Wavelength(cm)	3.10	5.3
Acquisition Mode	Strip-map Quad	Strip-map quad
Resolution (Rg x Az)	3x3m	3.3x2.3m
Mean Incidence Angle	38.79 degrees	37.685 degrees
Centre Latitude	32.34^0, 77.12^0	32.25^0, 77.26^0

Table 1-Data Specifications

3. METHEDOLOGY

3.1 Flow Diagram

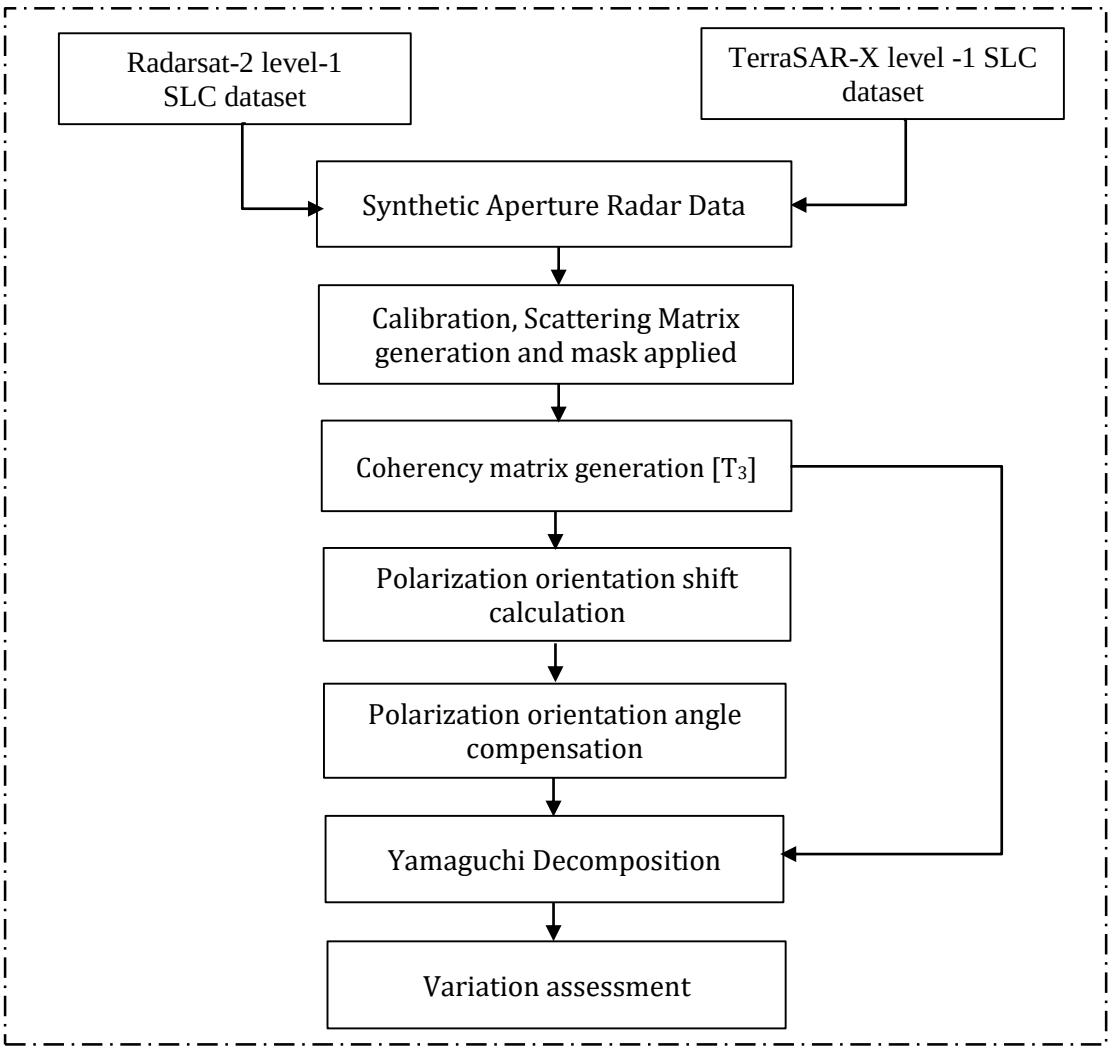

Figure 2-Methodology flow diagram

3.2 Detailed description of the steps in the methodological flow diagram: -

The Radarsat-2 and TerraSAR-X sensors level-1 SLC datasets were taken as input. The preprocessing of the datasets involved the calibration and the scattering matrix generation [S_2]. The scattering matrix gives the relation between the incident power E_I and the received backscattered power E_B. The 2x2 scattering matrix is generated to describe the quad-pol datasets having four polarization channels.

$$\mathrm{E_B} = \begin{bmatrix} S_{HH} & S_{HV} \\ S_{VH} & S_{VV} \end{bmatrix} E_I \qquad (1)$$

The coherency matrix T3 is generated to provide the second order scattering mechanism information. It is generated by the multiplication of scattering vector (K_P) in the pauli basis by its complex transconjugate ($K_p^{\dagger}$) of the scattering vector. The scattering vector K_P is defined in the equation 2 below.

$$k_p = \begin{bmatrix} (\mathrm{S_{HH}} + \mathrm{S_{VV}}) \\ (\mathrm{S_{HH}} - \mathrm{S_{VV}}) \\ (2S_{HV}) \end{bmatrix} \qquad (2)$$

The eq-3 shows the formation of the generated coherency matrix [T_3] :-

$$T_3 = k_p . k_p^{*T} = \frac{1}{2}\begin{bmatrix}(S_{HH}+S_{VV})\\(S_{HH}-S_{VV})\\(2S_{HV})\end{bmatrix}\begin{bmatrix}(S_{HH}+S_{VV})^* & (S_{HH}-S_{VV})^* & (2S_{HV})^*\end{bmatrix} \quad (3)$$

The output coherency matrix generated is shown in eq 4:-

$$T_3 = \begin{bmatrix}|(S_{HH}+S_{VV})|^2 & \frac{1}{2}(S_{HH}+S_{VV})(S_{HH}-S_{VV})^* & (S_{HH}+S_{VV})(2S_{HV})^*\\ \frac{1}{2}(S_{HH}-S_{VV})(S_{HH}+S_{VV})^* & \frac{1}{2}|(S_{HH}-S_{VV})|^2 & (S_{HH}-S_{VV})(2S_{HV})^*\\ (S_{HV})(S_{HH}+S_{VV})^* & (S_{HV})(S_{HH}-S_{VV})^* & 2|(S_{HV})|^2\end{bmatrix} \quad (4)$$

Yamaguchi decomposition technique represents the coherency matrix into sum of four scattering mechanisms- Surface scattering, Double bounce scattering Volume scattering and Helix scattering (Yamaguchi, Yajima, & Yamada, 2006).

$$< [T] >^{HV} = f_s [T]^{hv}_{surface} + f_d [T]^{hv}_{double} + f_v [T]^{hv}_{vol} + f_c < [T] >^{hv}_{helix} \quad (5)$$

Here Coherency matrix T_3 as the sum of powers in the surface scattering, double, volume and Helix scattering mechanisms in eq-6.

$$[T_3] = f_s \begin{bmatrix}1 & \beta^* & 0\\ \beta & |\beta|^2 & 0\\ 0 & 0 & 0\end{bmatrix} + f_d \begin{bmatrix}|\alpha|^2 & \alpha & 0\\ \alpha^* & 1 & 0\\ 0 & 0 & 0\end{bmatrix} + \frac{f_v}{2}\begin{bmatrix}2 & 0 & 0\\ 0 & 1 & 0\\ 0 & 0 & 1\end{bmatrix} + \frac{f_c}{2}\begin{bmatrix}0 & 0 & 0\\ 0 & 1 & \pm j\\ 0 & \pm j & 1\end{bmatrix} \quad (6)$$

Here β and α the surface bounce and the double bounce parameters, derived using X-Bragg's coefficient and Fresnel reflection coefficient respectively. f_s , f_d , ,f_v and f_c are the expansion coefficients. For more detailed study of this decomposition model (Yamaguchi et al., 2005) can be referred.

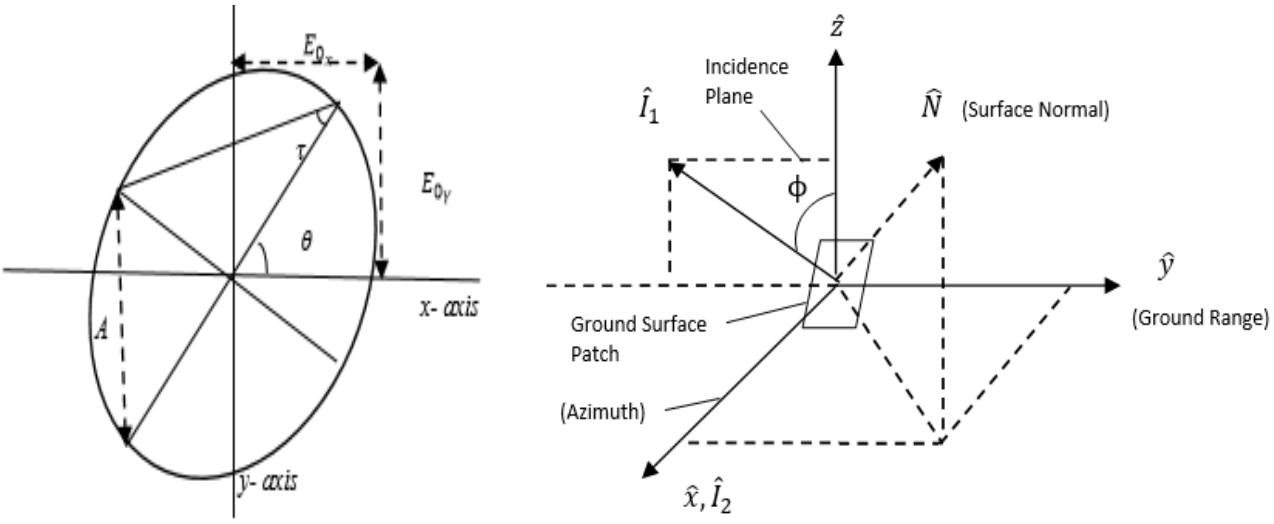

Figure 3-Polarization ellipse and the radar imaging geometry to relate the POA shift to the terrain slope (Iribe, Sato, & Member, 2007)

Fig-3 shows the polarization ellipse and the radar imaging geometry to relate the POA shift to the terrain slope. Here amplitude of the ellipse is represented as A and it is calculated as:-

$$A = \sqrt{E_{0x}^2 + E_{0y}^2} \tag{7}$$

The orientation angle in the ellipse is represented as θ. It is the angle formed between the semi-major axis and the horizontal axis. When the SAR data is collected for the rugged terrain the incidence plane is not perpendicular to the surface normal. Therefore the shift the incidence plane $(\hat{y}, \hat{z})$ is induced which causes its rotation by an angle θ. The induced POA shift depends on the azimuth and range slopes can be represented as (Lee & Ainsworth, 2011) eq-(8):-

$$tan\theta = \frac{tan\omega}{-tan\gamma\, cos\varphi + sin\varphi} \tag{8}$$

Here, θ is orientation angle shift, tanω is the azimuth slope, tanγ is a ground range slope and φ is radar look angle.

The Orientation angle φ can be easily computed as eq (9):-

$$\tan(-4\varphi) = \frac{-4Re(\langle(S_{HH} - S_{VV})S_{HV}^*\rangle)}{-\langle|S_{HH} - S_{VV}|^2\rangle + < |S_{HV}|^2 >} \tag{9}$$

This can be compensated by unwrapping the phase by adding π, as (Gupta, Kumar, & Pandey, 2016; Lee & Ainsworth, 2011)

$$\eta = \frac{1}{4}\left[\tan^{-1}\left(\frac{-4Re(\langle(S_{HH} - S_{VV})S_{HV}^*\rangle)}{-\langle|S_{HH} - S_{VV}|^2\rangle + < |S_{HV}|^2 >}\right) + \pi\right] \tag{10}$$

Where,

$$\theta = \begin{cases} \eta, \text{ if} & \eta \leq \frac{\pi}{4} \\ \eta - \frac{\pi}{2} \text{ if} & \eta > \frac{\pi}{4} \end{cases} \tag{11}$$

After the orientation angle correction the coherency matrix can be expressed as :-

$$[\bar{T}] = [U][T][U^T] \tag{12}$$

Where [U] is,

$$[U] = \begin{bmatrix} 1 & 0 & 0 \\ 0 & cos(2\theta) & \sin(2\theta) \\ 0 & -\sin(2\theta) & cos(2\theta) \end{bmatrix} \tag{13}$$

[$\bar{T}$] And [T] are the retrieved coherency matrices after and before rotation by Polarization orientation angle shift θ and [U] is the unitary rotation matrix which rotates the orientation angle by angle θ.

After following all the above mentioned steps the POA shift can be estimated and corrected successfully. This methodology is applied in both the datasets and the output is retrieved in next section.

4. RESULTS

Comparative analysis of both the datasets Radarsat-2/TerraSAR-X before and after POA shift compensation results of Yamaguchi Decomposition.

4.1 Yamaguchi decomposition analysis for Radarsat-2 dataset:-

The Yamaguchi decomposition for the RADARSAT-2 datasets was done and the RGB color composite images before and after POA shift was representing double, volume and the surface bounce scattering mechanisms respectively. It was found that volume scattering was overestimated and double bounce scattering was underestimated. Surface scattering was not effected much during the process of POA shift.

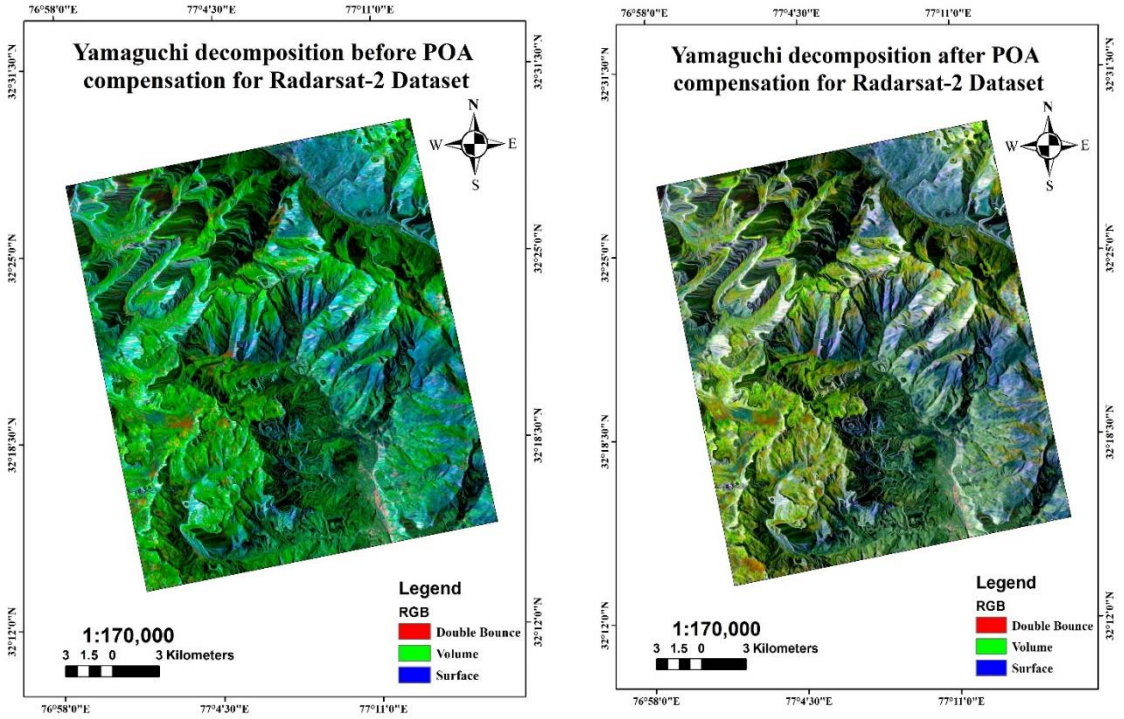

Figure 4-Radarsat-2 decomposed images before and after applying POA shift

4.2 Histogram analysis of POA shift in Radarsat-2 dataset:-

The range for the POA shift lies between -45^{0}and +45^0 The mean POA shift was -0.0016^0 and standard deviation in the POA shift was 11.95^0

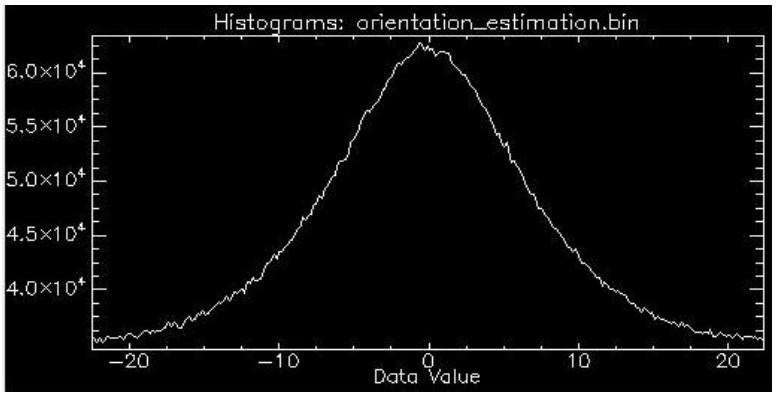

Figure 5-Histogram analysis of POA shift for Radarsat-2 dataset

4.3 Yamaguchi decomposition analysis for TerraSAR-X dataset

The Yamaguchi decomposition for the TerraSAR-X datasets was also done and the RGB color composite images before and after POA shift was representing double, volume and the surface bounce scattering mechanisms respectively. In TerraSAR-X datasets also the volume scattering was overestimated and double bounce scattering was underestimated. Here also, surface scattering was not effected much during the process of POA shift. This was also seen that the less frequency band TerraSAR-X datasets were less effected by the POA compensation compaired to the high wavelength Radarsat-2 datasets.

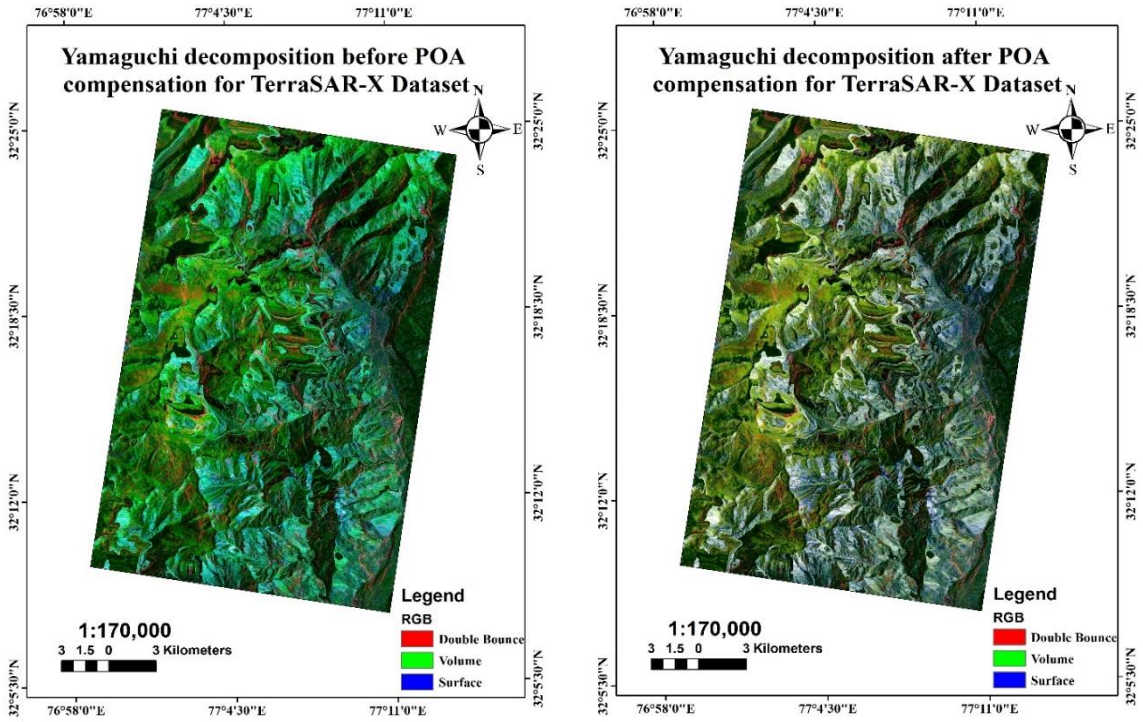

Figure 6-TerraSAR-X decomposed images before and after applying POA shift

4.4 Histogram analysis of POA shift in TerraSAR-X dataset:-

The POA shift range lies in between [-45^0,45^0]. The mean POA shift in degrees was -0.59 and standard deviation in the POA shift was 11.96.

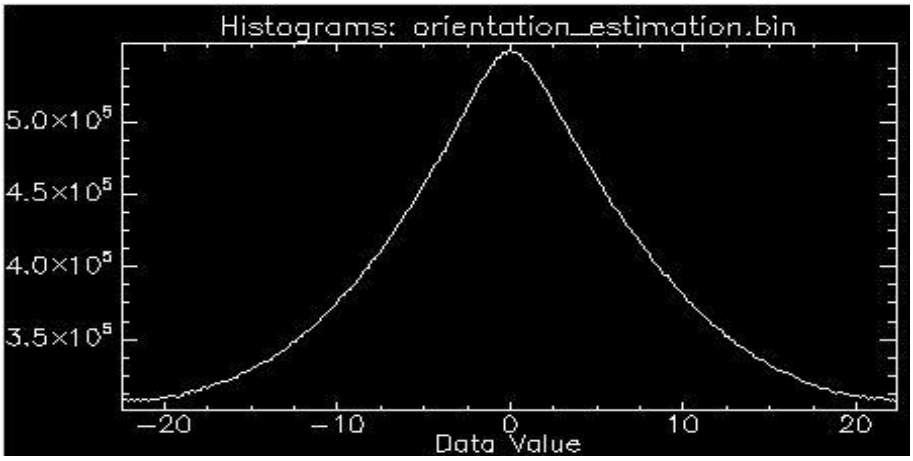

Figure 7-Histogram analysis of POA shift for TerraSAR-X dataset

4.5 Effect of POA shift on scattering mechanisms in RADARSAT-2 and TerraSAR-X datasets

The POA shift analysis was done over the specific scattering components in Radarsat-2 and TerraSAR-X datasets. The random ground sample points were taken in the study area to carry out this analysis.

4.5.1 Effect of POA shift on double bounce scattering

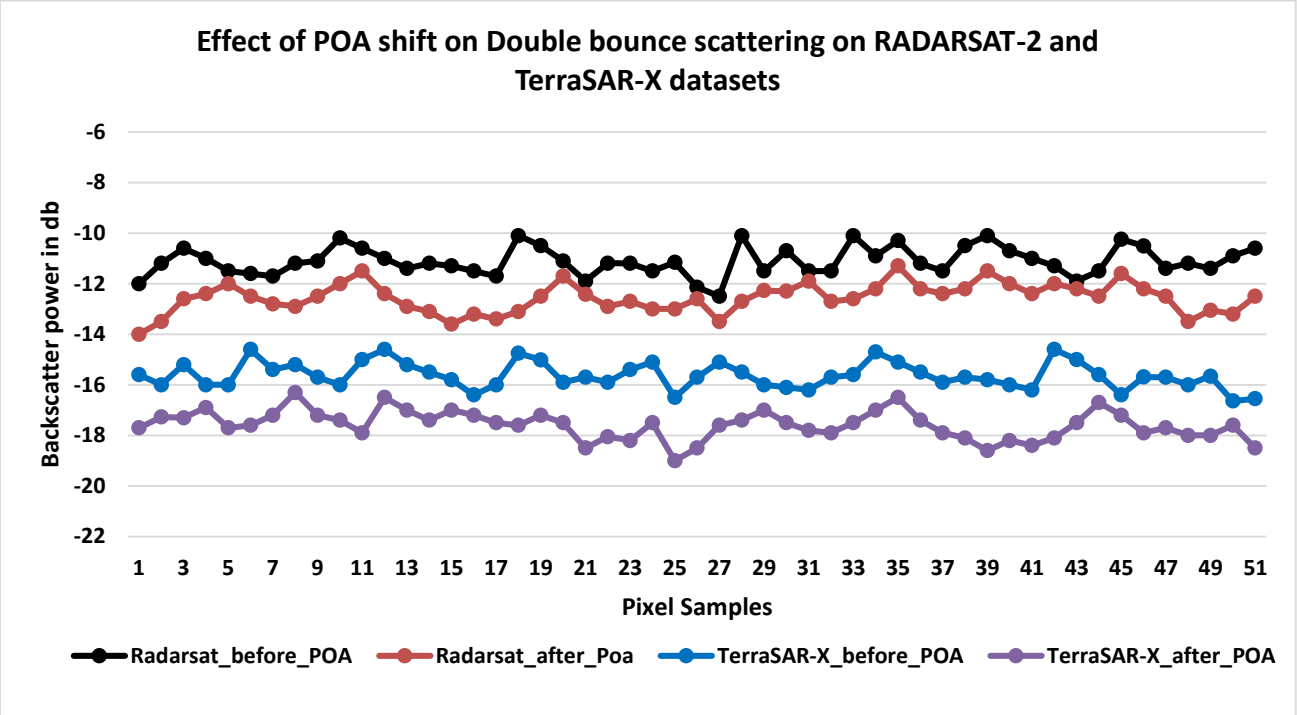

Figure 8-Effect of POA shift on double bounce scattering

4.5.2 Effect of POA shift on Volume scattering

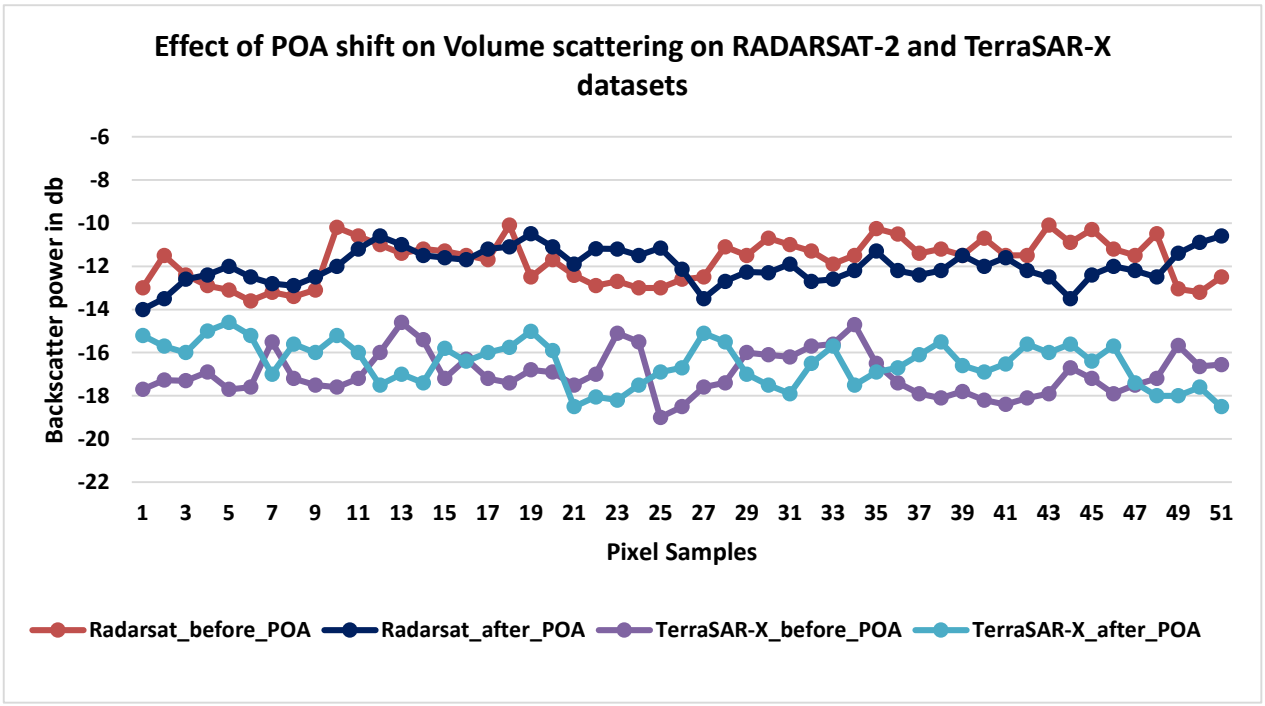

Figure 9-Effect of POA shift on Volume scattering

4.5.3 Effect of POA shift on Surface scattering

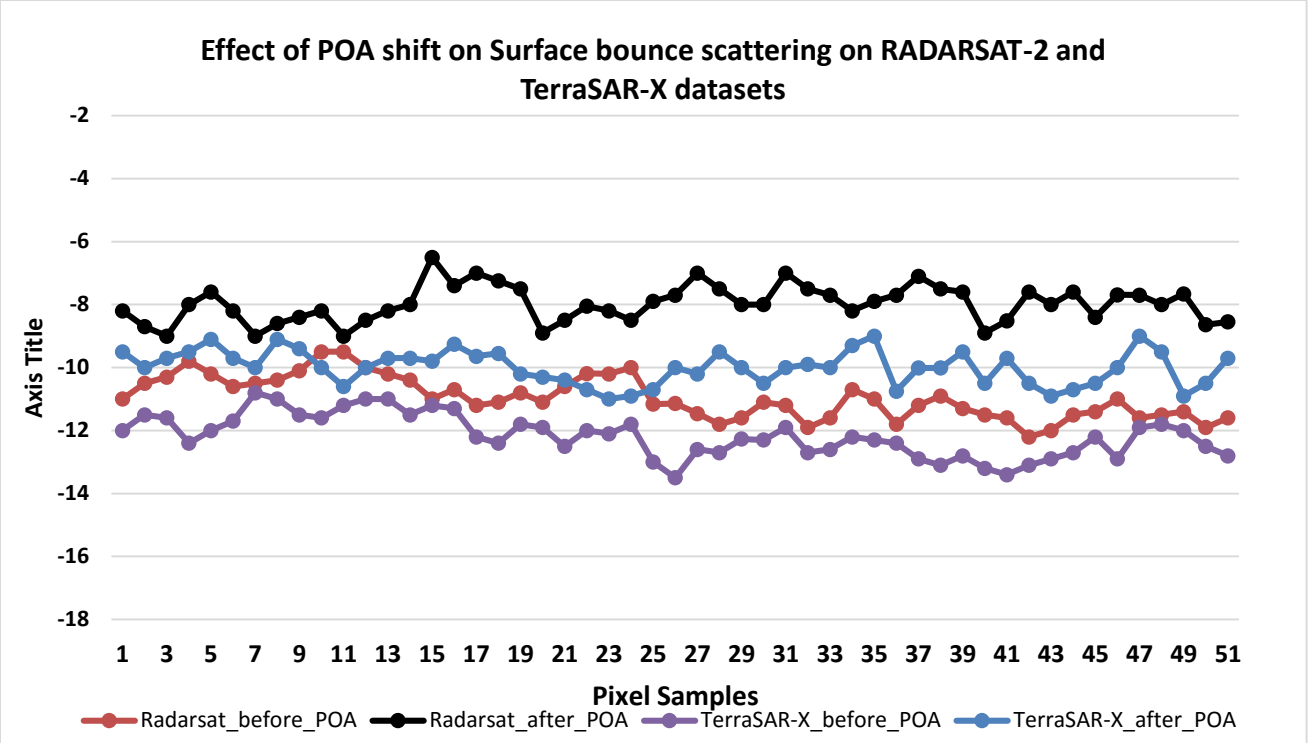

Figure 10-Effect of POA shift on Surface scattering

Fig 8, Fig- 9 and Fig-10 shows the POA shift effect on double bounce, volume and surface scattering mechanisms. The double bounce scattering component is mostly estimated as volume scattering components due to change in orientation angle plane. The volume scattering enhancement is seen due to false prediction of increase in randomness due to POA shift. The surface scattering is less effected due to POA shift. The effect of POA shift was found on Radarsat-2 dataset compaired to the TerraSAR-X datasets.

5. CONCLUSION

This study was effective in analyzing the effect of Polarization Orientation Angle (POA) shift on Synthetic aperture radar SAR data. The effect of the POA shift on different scattering mechanisms was analyzed and it was concluded that the POA shift causes the overestimation of the volume scattering components and less estimation of the double bounce scattering mechanisms. The POA shift effect on surface component is quite less as compaired to other scattering mechanisms. The POA shift effect was found more on the higher wavelength C-band Radarsat-2 datasets compaired to the X-band TerraSAR-X datasets. Hence it can be concluded that the datasets operating in the higher wavelength region are more effected by the POA shift.

6. REFERENCES

Freeman, A., & Durden, S. L. (1998). A three-component scattering model for polarimetric SAR data. *IEEE Transactions on Geoscience and Remote Sensing*, *36*(3), 963–973 https://doi.org/10.1109/.36.673687

Fung, A. K., & Chen, K. S. (2010). *Microwave Scattering and Emission Models for Users*. Artech House. Retrieved from https://books.google.co.in/books?id=blMmAgAAQBAJ

Gupta, A., Kumar, S., & Pandey, U. (2016). Effect of polarization orientation angle shift on X-band TDM SAR COSSC Product of TerraSAR-X and TanDEM-X, *9877*, 1–10. https://doi.org/10.1117/12.2223704

Iribe, K., Sato, M., & Member, S. (2007). Analysis of Polarization Orientation Angle Shifts by Artificial Structures. *IEEE Transactions on Geoscience and Remote Sensing*, *45*(11), 3417–3425. https://doi.org/10.1109/TGRS.2007.905973

Lee, & Ainsworth, T. L. (2011). The Effect of Orientation Angle Compensation on Coherency Matrix and Polarimetric Target Decompositions. *IEEE Transactions on Geoscience and Remote Sensing*, *49*(1), 849–852. https://doi.org/10.1109/TGRS.2010.2048333

Lee, J. Sen, Schuler, D. L., Ainsworth, T. L., Krogager, E., Kasilingam, D., & Boerner, W. M. (2002). On the estimation of radar polarization orientation shifts induced by terrain slopes. *IEEE Transactions on Geoscience and Remote Sensing*, *40*(1), 30–41. https://doi.org/10.1109/36.981347

Raney, R. K. (2007). Decomposition of hybrid- polarity SAR Data. *Proceedings of 3rd International Workshop on Science and Applications of SAR Polarimetry and Polarimetric SAR Interferometry (POLinSAR'07)*, 1–5.

Woodhouse, I. H. (2005). *Introduction to Microwave Remote Sensing*. Taylor & Francis. Retrieved from https://books.google.co.in/books?id=zuTUngEACAAJ

Yamaguchi, Y., Yajima, Y., & Yamada, H. (2006). A four-component decomposition of POLSAR images based on the coherency matrix. *IEEE Geoscience and Remote Sensing Letters*, *3*(3), 292–296. https://doi.org/10.1109/LGRS.2006.869986

Yamaguchi, Moriyama, T., Ishido, M., & Yamada, H. (2005). Four-component scattering model for polarimetric SAR image decomposition. *IEEE Transactions on Geoscience and Remote Sensing*, *43*(8), 1699–1706. https://doi.org/10.1109/TGRS.2005.852084